Improved photoswitching response times of MoS₂ field-effect transistors by stacking *p*-type copper phthalocyanine layer

Jinsu Pak,[1] Misook Min,[1,a)] Kyungjune Cho,[1] Der-Hsien Lien,[2] Geun Ho Ahn,[2] Jingon Jang,[1] Daekyoung Yoo,[1] Seungjun Chung,[1,b)] Ali Javey,[2] and Takhee Lee[1,b)]

[1]*Department of Physics and Astronomy and Institute of Applied Physics, Seoul National University, Seoul 08826, South Korea*
[2]*Electrical Engineering and Computer Sciences, University of California, Berkeley, California 94720, USA*

Photoswitching response times (rise and decay times) of a vertical organic and inorganic heterostructure with *p*-type copper phthalocyanine (CuPc) and *n*-type molybdenum disulfide (MoS₂) semiconductors are investigated. By stacking a CuPc layer on MoS₂ field effect transistors, better photodetection capability and fast photoswitching rise and decay phenomena are observed. Specifically, with a 2 nm-thick CuPc layer on the MoS₂ channel, the photoswitching decay time decreases from 3.57 s to 0.18 s. The *p*-type CuPc layer, as a passivation layer, prevents the absorption of oxygen on the surface of the MoS₂ channel layer, which results in a shortened photoswitching decay time because adsorbed oxygen destroys the balanced ratio of electrons and holes, leading to the interruption of recombination processes. The suggested heterostructure may deliver enhanced photodetection abilities and photoswitching characteristics for realizing ultra-thin and sensitive photodetectors. *Published by AIP Publishing.* [http://dx.doi.org/10.1063/1.4966668]

Recently, atomically thin transition metal dichalcogenides (TMDCs), such as molybdenum disulfide (MoS₂), molybdenum diselenide (MoSe₂), tungsten disulfide (WS₂), and tungsten diselenide (WSe₂), which have an intrinsic bandgap in contrast to zero-bandgap graphene, have attracted a great interest due to their potentials in various thin-film opto- and electronic applications.[1–5] Among the TMDC materials, MoS₂ has been widely investigated as a promising *n*-type 2-dimensional (2D) semiconductor material for realizing field effect transistor (FET) applications due to its excellent electrical properties, such as a high on/off ratio, near-ideal subthreshold swing, and reasonable carrier mobility.[6–9] Because of these remarkable advantages, many research groups have extensively studied MoS₂ in logic circuits, sensors, phototransistors, batteries, and memory applications.[9–13] In particular, its proper bandgap energy in the visible spectrum, which is determined by the thickness of MoS₂ (1.2–1.8 eV), suggests that it may be a promising material for photodetectors.[11,14,15] For better photodetection characteristics, several groups have recently introduced various materials to realize hybrid devices with *n*-type MoS₂ (see supplementary material, Table S1). Moreover, we have reported enhanced photoresponsivity properties of MoS₂ FETs by treating *p*-type copper phthalocyanine (CuPc) on the *n*-type MoS₂ channel surface, due to more activated creations of electron-hole pairs.[16]

In this paper, we report that CuPc treated MoS₂ FETs showed improved photoresponsivity and photoswitching response times concurrently. By stacking a 2 nm-thick *p*-type CuPc layer on the MoS₂ channel layer, the photoswitching rise and decay times decrease from 12.87 s to 5.07 s and

from 3.57 s to 0.18 s, respectively, showing better photoresponse behaviours than those of the pristine MoS₂ FETs.

For the fabrication of MoS₂ FETs, mechanically exfoliated bulk MoS₂ sheets were transferred to a heavily doped Si substrate with a 270 nm-thick thermally grown SiO₂ layer which can be used as a common back-gate electrode, as shown in Fig. 1. The MoS₂ sheet shown in Fig. 1(a) exhibited a thickness of ∼2.7 nm measured using an atomic force microscope (AFM), corresponding to a MoS₂ quadruple layer (MoS₂ single layer has a thickness of ∼0.65 nm). On the MoS₂ channel layers, titanium (Ti) (∼30 nm), which delivers a good contact property with the MoS₂ channel layer due to its low work function (∼4.33 eV), was deposited for the source and drain electrodes.[17] The fabrication processes are further described in the supplementary material in detail. Fig. 1(b) shows a schematic of the CuPc treated MoS₂ hybrid FET and the molecular structure of CuPc. We observed Raman shift peak positions of the multilayer MoS₂ and the CuPc layer (see supplementary material, Fig. S2), which indicated that the CuPc layer was well-deposited on the MoS₂ surface. To investigate the phenomena at the interface between *p*-type organic (CuPc) and *n*-type inorganic (MoS₂) layers, the measured electrical properties of the MoS₂ FETs with and without CuPc treatment (5 nm-thickness) were compared. Fig. 1(c) shows the transfer curves (drain current versus gate voltage, I_{DS}–V_{GS}) of the pristine MoS₂ (represented by filled circular symbols) and the CuPc treated MoS₂ (represented by open circular symbols) FETs measured with various source-drain voltages in vacuum (∼10⁻⁴ Torr) at room temperature. The inset plot in Fig. 1(c) shows the semi-logarithmic scale transfer curves. The mobility of the pristine and CuPc treated MoS₂ FETs was extracted to be ∼2.81 cm²/Vs and 1.73 cm²/Vs, respectively, from the following formula: $\mu = (dI_{DS} / dV_{GS}) \times [L/(WC_iV_{DS})]$, where L, W, and C_i denote the channel length (5.04 μm) and width (7.42 μm) of the FETs and the capacitance (1.3 × 10⁻⁸ F/cm²)

a)Present address: Department of Chemistry, Rice University, 6100 Main Street, Houston, Texas 77005, USA.
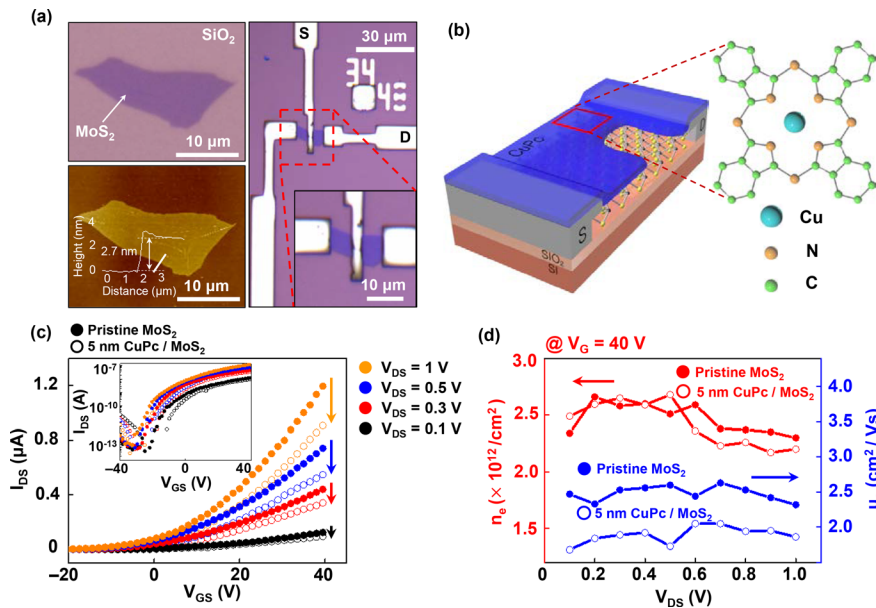b)Authors to whom correspondence should be addressed. Electronic addresses: seungjun@phya.snu.ac.kr and tlee@snu.ac.kr

FIG. 1. (a) Optical and AFM images of a MoS_2 FET. (b) Schematic of the CuPc treated MoS_2 FET and the molecular structure of CuPc. (c) Transfer characteristics of the pristine and 5 nm-CuPc treated MoS_2 FETs measured with various V_{DS} (transfer characteristics on the log scale are also presented in the inset). (d) The electron carrier concentration (n_e) and carrier mobility (μ_e) of both pristine MoS_2 and 5 nm-CuPc treated MoS_2 FETs as a function of V_{DS}.

between the channel and the heavily doped Si back-gate per unit area, respectively. The drain current decreased after introducing the 5 nm-CuPc treatment on the MoS_2 surface, as shown in Fig. 1(c). The decrease of the drain current can be explained by the decrease of the electron carrier concentration (especially when V_{DS} is larger than ~0.5 V) and the decrease of mobility after the CuPc treatment, as shown in Fig. 1(d). The reduced electron mobility originated from the scattering by the CuPc molecules acting as impurities at the interface between the MoS_2 and CuPc layers. This result is consistent with the previously reported result in that organic layers in organic/inorganic hybrid structures acted as a scattering center.[18]

The photoresponsive properties of MoS_2 FETs without and with the CuPc treatment were investigated using a 520 nm laser with a laser intensity of 40 mW and a spot radius of 5 mm at room temperature in ambient conditions.
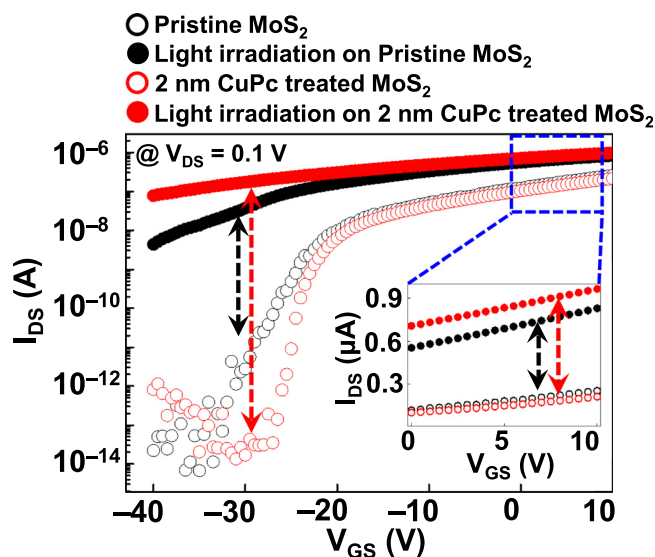

FIG. 2. Transfer characteristics of the pristine and 2 nm CuPc treated MoS_2 FET under dark and irradiated conditions at $V_{DS} = 0.1$ V (a magnified linear plot of I_{DS}–V_{GS} from $V_{GS} = 0$ V to 10 V is included in the inset).

Fig. 2 shows the transfer curves of the pristine MoS_2 FET (black symbols) and MoS_2 FET with the 2 nm-CuPc treatment (red symbols) measured at $V_{DS} = 0.1$ V. Under laser irradiation, electron-hole pairs can be generated in both the CuPc and MoS_2 layers by the photon energy because the energy of incident light (520 nm, 2.38 eV) is larger than the bandgap energy of the MoS_2 (~1.2 eV) and CuPc (~1.7 eV) layers. These photogenerated electron-hole pairs can contribute to the additional photocurrent, as represented by filled circular symbols. The black and red arrows in Fig. 2 indicate the photocurrent (I_{Ph}), which is I_{Light} (I_{DS} under irradiation) − I_{Dark} (I_{DS} in the dark). These results clearly showed that better photodetection was observed for the CuPc treated MoS_2 FET when compared with the pristine MoS_2 FET because photogenerated electron-hole pairs can be separated easily at the p-n interface and photogenerated electrons and holes in the CuPc layer can contribute to the photocurrent. Hence, the photocurrent and the current ratio after irradiation (I_{Light}/I_{Dark}) were amplified from 3.7×10^{-8} A to 1.7×10^{-7} A and from 1.3×10^4 to 1.0×10^7, respectively, at $V_{DS} = 0.1$ V and $V_{GS} = -30$ V, as shown in Fig. 2. We presented the gate voltage dependence of photoresponsivity (R) and detectivity (D^*), which are primary parameters for evaluating photodetection abilities. The characteristics of our devices were compared with those of other MoS_2 based photoresponsive devices (see supplementary material, Fig. S4 and Table S1).

In addition, the photoswitching rise (τ_{rise}) and decay (τ_{decay}) times of the pristine and CuPc treated MoS_2 FETs were investigated. Here, τ_{rise} is defined as the time required for the current change from 10% to 90% of the maximum amplitude, and τ_{decay} is the time at which the amplitude decreases to $1/e$ times from its initial value, where e is the constant based on the natural logarithm. Fig. 3 shows a plot of the normalized photoswitching data, demonstrating the rise and decay dynamics under 520 nm laser irradiation under ambient conditions for 20 s, measured at $V_{GS} = -40$ V and $V_{DS} = 0.1$ V. After depositing a 2 nm-CuPc layer on the MoS_2 channel, the rise and decay times
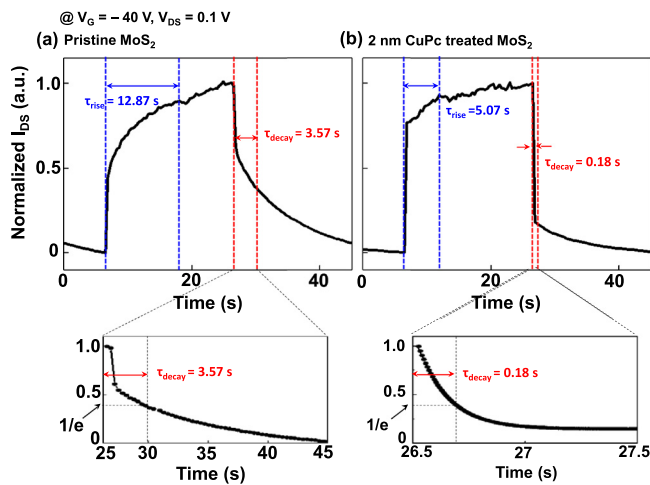
FIG. 3. Normalized photoswitching results of (a) pristine and (b) 2 nm CuPc treated MoS$_2$ FETs at $V_{GS} = -40$ V and $V_{DS} = 0.1$ V.

decreased from 12.87 s to 5.07 s and from 3.57 s to 0.18 s, respectively. In particular, the decay time was drastically shortened to almost 5% of the original value after the CuPc surface treatment. As the randomly localized potential fluctuations in MoS$_2$ originated from sulfur vacancies, chemical impurities, and unstable contact resistance with substrates that can also contribute to long recombination lifetime,[19] the decay time in the 0.1 s range was still observed after turning off irradiation even though the MoS$_2$ channel surface was covered with the CuPc layer to improve photoresponse times. Further shortened photoresponse times would be expected by inserting a hBN interlayer or using a laser with extremely low intensity during the measurement. We also investigated the CuPc thickness dependence of the rise and decay times, represented by blue and red symbols, respectively, in Fig. 4. This result showed that the rise and decay times decreased rapidly up to 2 nm CuPc deposition and then became saturated as the CuPc thickness was further increased. These improved photoswitching response times by the CuPc surface treatment can be explained by the relationship between free carriers and absorbed oxygen at the surface. The
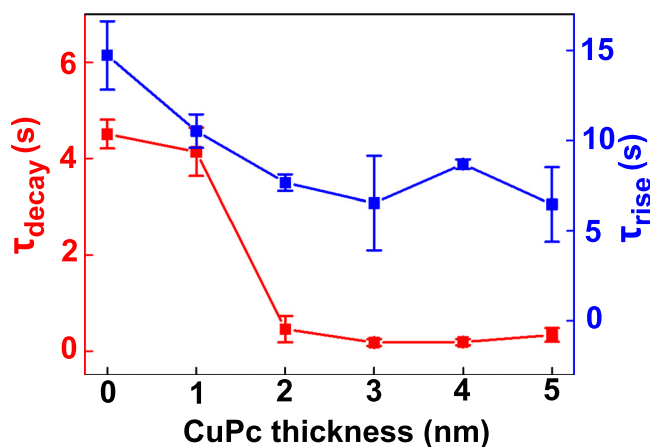
photoswitching mechanisms of the pristine and CuPc treated MoS$_2$ FETs are described in Fig. 5.

For the pristine MoS$_2$ FETs, oxygen molecules are attached on the MoS$_2$ surface with trapping electrons [O$_2$ + e → O$_2^-$], which causes a significant reduction of the MoS$_2$ channel conductance, as shown in Fig. 5(a). In the MoS$_2$ FETs, oxygen molecules are physically adsorbed on the MoS$_2$ channel surface with a weak binding energy (this is explained in the supplementary material in detail). Under laser irradiation, adsorbed oxygen can be detached due to the recombination between trapped electrons and photogenerated holes [O$_2^-$ + h → O$_2$], which results in an increase in the conductance of the MoS$_2$ channel (Fig. 5(b)). In contrast to photogenerated holes, which move to the surface to recombine with trapped electrons, photogenerated electrons mainly contribute additional current unless they are trapped again by oxygen adsorbed on the surface (Fig. 5(b)). These photogenerated electrons accumulate in the MoS$_2$ channel gradually until the adsorption and desorption processes of oxygen molecules reach the equilibrium state, which explains why the drain current continuously increased until the saturation region during laser irradiation (see Fig. 3(a)). In this manner, the pristine MoS$_2$ FETs have a long rise time through repeated absorption and desorption processes until reaching the equilibrium state during laser irradiation. If

FIG. 4. Decay (τ_{decay}) and rise times (τ_{rise}) versus CuPc thicknesses from 0 to 5 nm. The symbols and error bars indicate average values and standard deviations from three measurements.
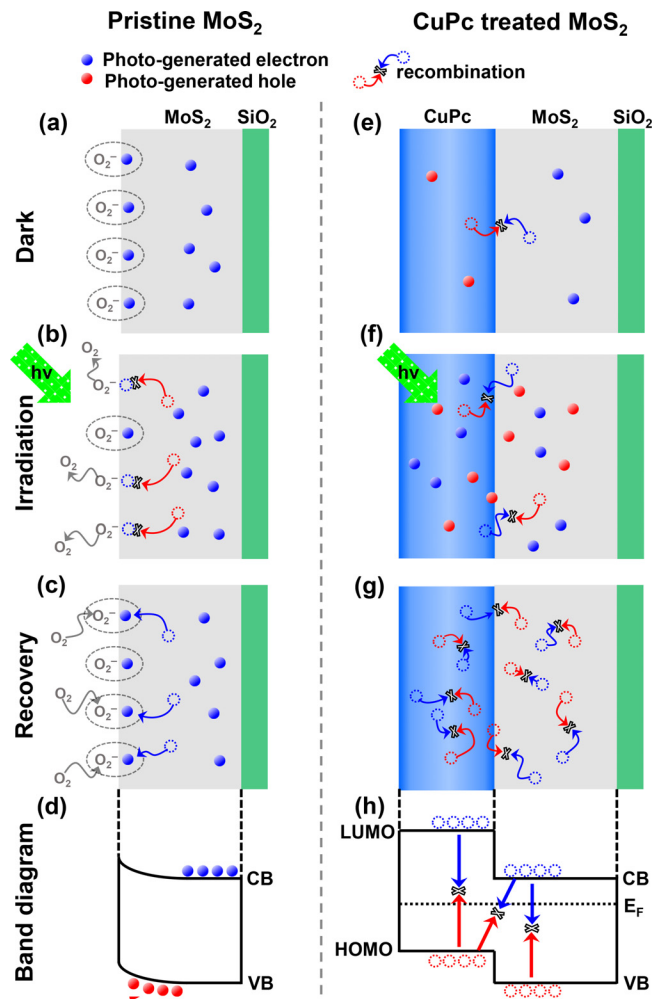

FIG. 5. Photoswitching processes and band diagram (a)–(d) before the CuPc treatment and (e)–(h) after the CuPc treatment.

light irradiation is turned off, much more electrons remain than holes because many holes have already recombined with the trapped electrons by oxygen molecules at the MoS_2 surface. Although holes can recombine with electrons right after turning off laser irradiation, the electrons, which are not recombined, still remain in the MoS_2 channel. In other words, unpaired electrons are gradually trapped at the surface and impede the fast photoswitching decay process, as shown in Fig. 5(c). These results are consistent with a previous report, in which the authors showed that absorbed oxygen can destroy the ratio of electrons and holes and lead to a long decay time.[20] Fig. 5(d) shows the energy band diagram with oxygen molecules adsorbed on the MoS_2 surface, which results in band bending near the surface by the reduced electron density. Due to the band bending near the surface, the electron-hole pairs are separated and cannot recombine well, which results in a long decay time. In summary, the absorbed oxygen molecules cause long photoswitching rise and decay times in the untreated MoS_2 FET because oxygen molecules trap electrons, leading to less recombination after the irradiation is turned off.

On the contrary, oxygen molecules cannot be adsorbed on the MoS_2 surface in the CuPc treated MoS_2 FET. Note that the major carriers of each layer can recombine at the interface in the dark state due to the difference of carrier concentrations, as shown in Fig. 5(e). During laser irradiation, the drain current can reach the saturation region rapidly because of negligible absorbed oxygen molecules on the MoS_2 channel, which results in a short rise time (see Fig. 3(b)). Then, additionally photogenerated electrons and holes accumulate continuously during laser irradiation, which means that the number of remaining electrons is comparable to that of the remaining holes during laser irradiation. Therefore, the electrons and holes can recombine quickly upon turning off irradiation due to the comparable numbers of electrons and holes, resulting in a fast decay time (Fig. 5(g)). Moreover, fast recombination is allowed by the band to band recombination in each layer of the CuPc and MoS_2 as well as the Langevin recombination between the CuPc and MoS_2 layers, as shown in Fig. 5(h). From these analyses, the CuPc surface treatment, working as a passivation layer, can be an effective method for shortening photoswitching response times against oxygen.

In summary, we examined the photodetection and photoswitching response times of MoS_2 FETs by stacking a CuPc layer. By depositing a CuPc layer on the MoS_2 channel, we observed enhanced photoresponsivity compared to pristine MoS_2 FETs. In particular, the photoswitching rise and decay characteristics of the CuPc-treated MoS_2 FETs were noticeably improved. In particular, the decay time was shortened from 3.57 s to 0.18 s at $V_{DS} = 0.1$ V and $V_G = -40$ V after introducing a 2 nm-thick CuPc layer on the MoS_2 channel. The CuPc surface treatment created a *p-n* vertical interface with the MoS_2 channel layer, resulting in enhanced photoresponsivity, and this treatment also played a role in creating a passivation layer against oxygen, which induced fast photoswitching response times. Our results may

provide a promising route for ultra-thin and highly sensitive MoS_2 photoswitching applications.

See supplementary material for fabrication process in detail, and Raman shift peak positions in Fig. S1 and S2. Fig. S3 shows transfer curve of a MoS_2 FET in ambient and vacuum environments. Gate voltage dependence of detectivity and photoresponsivity is indicated in Fig. S4, and optical characteristics of our device were compared with those of other MoS_2 based hybrid devices in Table S1.

[1]Q. H. Wang, K. Kalantar-Zadeh, A. Kis, J. N. Coleman, and M. S. Strano, Nat. Nanotechnol. **7**, 699 (2012).
[2]F. Xia, H. Wang, D. Xiao, M. Dubey, and A. Ramasubramaniam, Nat. Photonics **8**, 899 (2014).
[3]Y. Ye, Z. J. Wong, X. Lu, X. Ni, H. Zhu, X. Chen, Y. Wang, and X. Zhang, Nat. Photonics **9**, 733 (2015).
[4]J. S. Ross, P. Klement, A. M. Jones, N. J. Ghimire, J. Yan, D. G. Mandrus, T. Taniguchi, K. Watanabe, K. Kitamura, W. Yao, D. H. Cobden, and X. Xu, Nat. Nanotechnol. **9**, 268 (2014).
[5]X. Duan, C. Wang, J. C. Shaw, R. Cheng, Y. Chen, H. Li, X. Wu, Y. Tang, Q. Zhang, A. Pan, J. Jiang, R. Yu, Y. Huang, and X. Duan, Nat. Nanotechnol. **9**, 1024 (2014).
[6]B. Radisavljevic, A. Radenovic, J. Brivio, V. Giacometti, and A. Kis, Nat. Nanotechnol. **6**, 147 (2011).
[7]S. Kim, A. Konar, W.-S. Hwang, J. H. Lee, J. Lee, J. Yang, C. Jung, H. Kim, J.-B. Yoo, J.-Y. Choi, Y. W. Jin, S. Y. Lee, D. Jena, W. Choi, and K. Kim, Nat. Commun. **3**, 1011 (2012).
[8]C. D. English, G. Shine, V. E. Dorgan, K. C. Saraswat, and E. Pop, Nano Lett. **16**, 3824 (2016).
[9]H. Wang, L. Yu, Y.-H. Lee, Y. Shi, A. Hsu, M. L. Chin, L.-J. Li, M. Dubey, J. Kong, and T. Palacios, Nano Lett. **12**, 4674 (2012).
[10]Y. Tong, Z. Lin, J. T. L. Thong, D. S. H. Chan, and C. Zhu, Appl. Phys. Lett. **107**, 123105 (2015).
[11]H. S. Lee, S.-W. Min, Y.-G. Chang, M. K. Park, T. Nam, H. Kim, J. H. Kim, S. Ryu, and S. Im, Nano Lett. **12**, 3695 (2012).
[12]L. Hu, Y. Ren, H. Yang, and Q. Xu, ACS Appl. Mater. Interfaces **6**, 14644 (2014).
[13]E. Zhang, W. Wang, C. Zhang, Y. Jin, G. Zhu, Q. Sun, D. W. Zhang, P. Zhou, and F. Xiu, ACS Nano **9**, 612 (2015).
[14]K. F. Mak, C. Lee, J. Hone, J. Shan, and T. F. Heinz, Phys. Rev. Lett. **105**, 136805 (2010).
[15]X. Wang, P. Wang, J. Wang, W. Hu, X. Zhou, N. Guo, H. Huang, S. Sun, H. Shen, T. Lin, M. Tang, L. Liao, A. Jiang, J. Sun, X. Meng, X. Chen, W. Lu, and J. Chu, Adv. Mater. **27**, 6575 (2015).
[16]J. Pak, J. Jang, K. Cho, T.-Y. Kim, J.-K. Kim, Y. Song, W.-K. Hong, M. Min, H. Lee, and T. Lee, Nanoscale **7**, 18780 (2015).
[17]I. Popov, G. Seifert, and D. Tomanek, Phys. Rev. Lett. **108**, 156802 (2012).
[18]Y. Xu, O. T. Hofmann, R. Schlesinger, S. Winkler, J. Frisch, J. Niederhausen, A. Vollmer, S. Blumstengel, F. Henneberger, N. Koch, P. Rinke, and M. Scheffler, Phys. Rev. Lett. **111**, 226802 (2013).
[19]Y.-C. Wu, C.-H. Liu, S.-Y. Chen, F.-Y. Shih, P.-H. Ho, C.-W. Chen, C.-T. Liang, and W.-H. Wang, Sci. Rep. **5**, 11472 (2015).
[20]Y. Li, F. D. Valle, M. Simonnet, I. Yamada, and J.-J. Delaunay, Appl. Phys. Lett. **94**, 023110 (2009).